

Nanotomography with enhanced resolution using bimodal atomic force microscopy

C. Dietz,^{1,a)} M. Zerson,¹ C. Riesch,¹ A. M. Gigler,² R. W. Stark,² N. Rehse,¹ and R. Magerle^{1,b)}

¹*Chemische Physik, Technische Universität Chemnitz, Reichenhainer Str. 70, 09107 Chemnitz, Germany*

²*Center for Nanoscience and Department of Earth and Environmental Science, Ludwig-Maximilians-Universität München, Theresienstraße 41/II, 80333 München, Germany*

(Received 18 February 2008; accepted 17 March 2008; published online 9 April 2008)

High resolution volume images of semicrystalline polypropylene were obtained by stepwise wet-chemical etching followed by atomic force microscopy of the specimen. Enhanced signal-to-noise ratio and spatial resolution were achieved by using the second flexural eigenmode of the cantilever for phase imaging while the amplitude of the first mode was used as feedback signal. The energy dissipated between the tip and the sample revealed characteristic differences between the crystalline and the amorphous regions of the polypropylene after etching, indicating the presence of a thin (<10 nm thick) amorphous layer on top of crystalline regions. © 2008 American Institute of Physics. [DOI: 10.1063/1.2907500]

Atomic force microscopy¹ (AFM) has become a widely used tool for the investigation of all kinds of materials. The limitation of AFM to image only surfaces has been overcome with nanotomography.² This layer-by-layer imaging technique allows volume imaging by combining AFM imaging with stepwise ablating the specimen with plasma etching,² wet-chemical etching,³ or chemomechanical polishing.⁴ The lateral force of the AFM tip on the sample has been decreased using dynamic or tapping mode AFM.⁵ By oscillating the tip, the contact time between the specimen and the tip is drastically reduced which in turn decreases potentially destructive forces on the specimen and the tip. Different variants of dynamic AFM have been developed which provide material specific contrast and means for probing the specimen's surface properties.⁶ Rodríguez and García⁷ have shown that the second mode of the cantilever oscillation has a sensitivity to surface force variations better than 10^{-11} N. Higher eigenmodes of the vibrating cantilever can enhance the signal-to-noise ratio and provide a better spatial resolution (as demonstrated on SiO₂)⁸ as well as different contrast (as demonstrated on polydiethylsiloxane).⁹ In this letter, we demonstrate high resolution nanotomography of semicrystalline polypropylene using bimodal AFM.⁷

Cleveland *et al.*¹⁰ and Tamayo and García¹¹ have proposed an analytical expression for power loss and energy dissipation due to the tip-sample interaction in tapping mode AFM. The shape of the dissipation curve, i.e., the energy dissipated between the tip and the sample as a function of the cantilever's oscillation amplitude allows the identification of the dissipation mechanism at the nanoscale.¹²

To study mechanical properties and to identify dissipation processes of the elastomeric polypropylene (ePP) surface before and after wet-chemical etching, we measured amplitude-phase-distance (APD) curves by vibrating the cantilever at its resonance frequency while approaching toward the sample. The cantilever's vibration amplitude A and phase shift Φ with respect to the excitation were re-

corded as a function of the tip-sample separation. From these data, the energy E_{dis} dissipated per oscillation cycle can be calculated^{10,11} by

$$E_{\text{dis}} = E_{\text{ext}} - E_{\text{med}} = \frac{\pi k A}{Q} \left(A_0 \sin \phi - \frac{A \omega}{\omega_0} \right), \quad (1)$$

where E_{ext} and E_{med} are the excitation energy and the energy dissipated into the medium, respectively, k is the force constant, Q is the quality factor of the cantilever, ω is the excitation frequency, and ω_0 is the cantilever's resonance frequency. E_{dis} is plotted versus the ratio A/A_0 between the oscillation amplitude A and the free amplitude A_0 . For measurements of dissipation curves, we used a NanoWizard I AFM (JPK Instruments AG, Berlin, Germany) and silicon cantilevers (Pointprobe® NCH from NanoWorld AG, Neuchâtel, Switzerland) with $\omega_0 \approx 284$ kHz, $Q \approx 200$, and $k \approx 9.5$ N/m at a free amplitude of $A_0 \approx 35$ –40 nm.

For bimodal AFM imaging a MultiMode™ AFM (Veeco Instruments Inc., Santa Barbara, USA) was used. The first two flexural eigenmodes ($f_1 \approx 122$ kHz, $f_2 \approx 758$ kHz) of the cantilever (SEIHR-SPL from Nanosensors, Germany) were mechanically excited. The first eigenmode was excited to a free amplitude A_0 of about 30 nm. An amplitude ratio between the two modes of $A_2/A_1 = 0.2$ turned out to give the best contrast for the studied polymer. The setpoint ratio A_1/A_0 was in the range of 0.35–0.72. It was adjusted for best contrast and stable imaging conditions. The cantilever deflection signal was analyzed by a dual reference lock-in amplifier of a custom-built bimodal control unit similar to that in Ref. 13. The amplitude of the first eigenmode was the signal for the z feedback whereas the phase signal of the second eigenmode provided compositional contrast.⁷

We studied ePP with a weight-average molecular weight $M_w = 160$ kg mol⁻¹ and a [mmmm]-pentade (m = meso conformation) content of 36%.¹⁴ A 150 nm thick polymer film on a gold coated silicon substrate was prepared by dip coating from a 5 mg/ml ePP solution in decaline. The film thickness before and after the last etching step was measured as previously described.³ We sequentially removed thin layers of about 10 nm thickness of the polymer by wet-chemical

^{a)}Electronic mail: christian.dietz@s2005.tu-chemnitz.de.

^{b)}Electronic mail: robert.magerle@physik.tu-chemnitz.de.

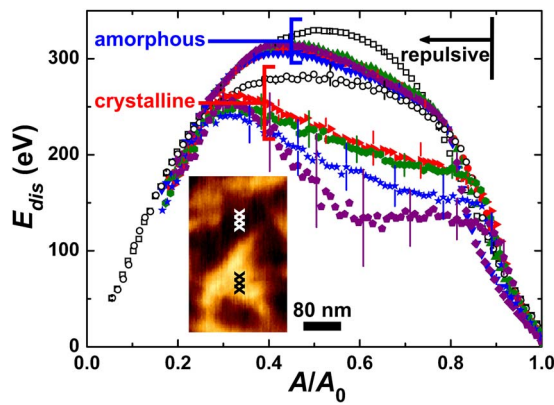


FIG. 1. (Color online) Averaged dissipation curves measured on amorphous and on crystalline regions of ePP before (open symbols) and after 1, 5, 10, and 15 etching steps (closed symbols, red, green, blue, and purple, respectively). The inset shows the corresponding phase image (phase range 0° – 31°). The positions where APD curves were measured are marked with crosses. The black arrow indicates the transition from the attractive to the repulsive regime. For clarity, error bars are only shown for every tenth data point.

etching with a solution of 50 mg/ml potassium permanganate in 30 wt % sulfuric acid for 1 min followed by rinsing first with 10 wt % sulfuric acid then with hydrogen peroxide, pure water, and finally with acetone. After etching, the sample was remounted into the AFM and the position of interest was imaged. The obtained stack of images was post-processed including flattening and filtering, combined to a volume image, and visualized as previously described.^{3,15,16}

For the investigation of the influence of the etching procedure on the mechanical properties of the polymer, we measured dissipation curves on ePP after several etching steps (Fig. 1). The upper five curves enclosed by the blue bracket correspond to the dissipation curves obtained on an amorphous region of ePP before ablation, and after 1, 5, 10, and 15 etching steps, respectively. The lower curves marked with the red bracket were correspondingly measured on crystalline regions. The data points were obtained by averaging the three APD curves of each polymer region measured at the positions indicated by the crosses in the inset. The corresponding standard deviation is indicated by the error bars for every tenth data point. The energy dissipation was determined from APD curves measured at about 50 different positions on amorphous regions and scattered by 10%. On crystalline regions, the scatter was 40%. Here, the dissipated energy strongly depends on how close the AFM tip was located to the center of the crystalline region during the APD measurement. The amount of energy dissipation was always lower on the crystalline part than on the amorphous one. This observation is explained by the higher stiffness of the crystalline regions of ePP. On the amorphous region, the curves measured after the first and the subsequent etching steps were all very similar to the curve measured prior to etching. The variation was within the scatter mentioned above. The shape of the curves resembled a dissipation process in which viscoelastic forces between tip and sample prevail.¹² The slight decrease in the maximum amount of energy can be ascribed to a change of the tip apex, which is likely to become blunter during the measurement. There was no drastic change neither in the amount of energy dissipation nor in the shape of the curves. Thus, we conclude that the mechanical properties on amorphous regions of the surface were not

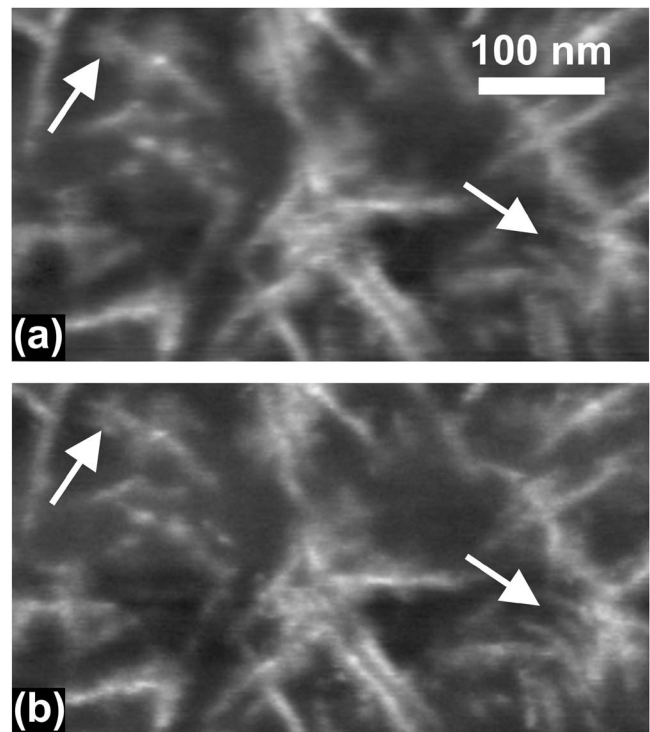


FIG. 2. Comparison of phase images of the (a) first and the (b) second eigenmode after the first etching step on ePP. The arrows indicate features which can only be resolved in the second eigenmode image (b). (phase range 0° – 36° .)

significantly altered during etching. The dissipation curve measured on the crystalline region before etching was very similar to dissipation curves measured on the amorphous regions. After the first etching, the curve shape changed and the maximum amount of dissipated energy decreased by about $\frac{1}{3}$. We attribute this effect to a decrease of viscoelastic dissipation and an increase of the stiffness of the surface. Both indicates the presence of a thin (<10 nm thick) amorphous layer on top of the crystalline region, which was removed during the first etching step. This finding is in accordance with Ref. 17, where a 3 nm thick amorphous layer was found on crystalline regions. After the subsequent etching steps, the variation of the curves remained within the typical scatter.

The AFM height images (not shown) measured on ePP before and after the subsequent etching steps looked similar to those in Ref. 3 with a typical roughness (peak to valley) of about 4 nm before and about 30 nm after 13 etching steps. The indentation of the AFM tip into the sample surface was determined by following the procedure in Ref. 18. The maximum penetration depth was 5 ± 2 nm at the lowest setpoint ratio $A_1/A_0=0.35$ on crystalline and amorphous regions. Similar values were obtained earlier.³

In order to enhance resolution and contrast and thus to improve the resulting nanotomography volume image, we applied the bimodal concept for imaging. Figure 2 shows a comparison between the phase image of (a) the first and (b) the second eigenmode measured with bimodal excitation after the first etching step. Dividing the average phase value of all data points within one image by its standard deviation clearly showed that the second eigenmode phase images exhibited (on average) an 1.3 ± 0.4 times higher signal-to-noise ratio than those of the first eigenmode phase. This particular

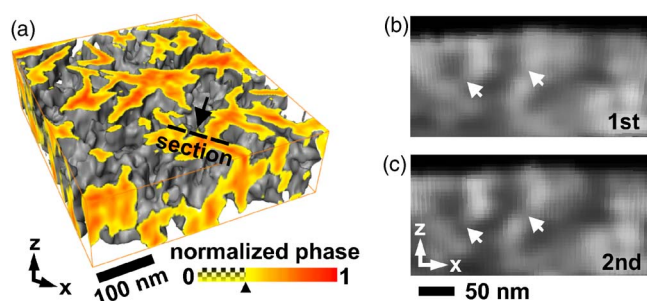


FIG. 3. (Color online) (a) Nanotomography volume image ($512 \times 512 \times 14$ voxels) of ePP displayed as isosurface. The image was captured by using bimodal AFM where the height image is simultaneously measured with the second eigenmode phase signal. The threshold between amorphous and crystalline phase was set to 0.32 (see marker at the color bar). The boundary box faces were colored according to the phase values. (b) Cross section through the x - z plane indicated in (a) for the first eigenmode volume image. (c) Same as (b) for the second eigenmode volume image.

relation was found for the whole sequence of images. The only exception was the very first image which was captured on the native surface just before the start of the etching process. The reduced resolution observed on the native surface is attributed to the thin amorphous layer covering the specimen. This surface layer screened the properties of the layer beneath so that the motion of the cantilever's second eigenmode was less sensitive to material variations beneath this layer. Comparing the images of the etching sequence obtained with both eigenmodes, the phase image of the first mode always appeared a bit more blurred compared to that of the second eigenmode. The second eigenmode phase images showed more sharply defined features. The white arrows in Fig. 2 indicate positions where two or more crystallites can hardly be distinguished in the first eigenmode phase image [Fig. 2(a)] but are clearly visible in the second eigenmode image [Fig. 2(b)]. This enhanced sensitivity to compositional changes has been predicted by Rodríguez and García⁷ and observed by Stark *et al.*⁸ on SiO₂ surfaces. This effect was seen in all images of our etching series which is a great advantage for nanotomography imaging. The resulting volume image which was reconstructed from the series of second eigenmode phase data is shown in Fig. 3(a). The black arrow indicates the position of the cross section through the x - z plane that is shown in Figs. 3(b) and 3(c). The white arrows mark the positions where gaps between crystals appear clearer in the second eigenmode volume image [Fig. 3(c)] than in the first eigenmode image [Fig. 3(b)].

In summary, we have shown that energy dissipation curves allow for clearly distinguishing between amorphous

and crystalline regions of semicrystalline polypropylene. On the latter, an <10 nm thick amorphous layer was found which was removed by wet-chemical etching. After etching, considerably less energy was dissipated on the rather stiff crystalline regions than on the embedding amorphous phase. Here, the shape of dissipation curves indicates viscoelastic dissipation between the tip and the sample. Even after having removed 140 nm of the polymer by stepwise wet-chemical etching, the shape of the curves remained almost constant. This shows that the mechanical properties of the polypropylene surface were not significantly changed by the etching procedure. Furthermore, we demonstrated that the spatial resolution and the signal-to-noise ratio of the nanotomography images can be enhanced by using bimodal AFM. We expect that the structural investigation of other multicomponent materials will also benefit from the combination of nanotomography with bimodal imaging.

This work was financially supported by the European Commission (FORCETOOL, NMP4-CT-2004-013684) and the VolkswagenStiftung.

- ¹G. Binnig, C. F. Quate, and Ch. Gerber, *Phys. Rev. Lett.* **56**, 930 (1986).
- ²R. Magerle, *Phys. Rev. Lett.* **85**, 2749 (2000).
- ³N. Rehse, S. Marr, S. Scherdel, and R. Magerle, *Adv. Mater. (Weinheim, Ger.)* **17**, 2203 (2005).
- ⁴M. Göken, R. Magerle, M. Hund, and K. Durst, *Prakt. Metallogr.* **35**, 257 (2004).
- ⁵Q. Zhong, D. Inniss, K. Kjoller, and V. B. Elings, *Surf. Sci. Lett.* **290**, L688 (1993).
- ⁶For a recent review, see R. García and R. Pérez, *Surf. Sci. Rep.* **47**, 197 (2002).
- ⁷T. R. Rodríguez and R. García, *Appl. Phys. Lett.* **84**, 449 (2004).
- ⁸R. W. Stark, T. Drobek, and W. M. Heckl, *Appl. Phys. Lett.* **74**, 3296 (1999).
- ⁹S. N. Magonov, V. Elings, and V. S. Papkov, *Polymer* **38**, 297 (1997).
- ¹⁰J. P. Cleveland, B. Anczykowski, A. E. Schmid, and V. B. Elings, *Appl. Phys. Lett.* **72**, 2613 (1998).
- ¹¹J. Tamayo and R. García, *Appl. Phys. Lett.* **73**, 2926 (1998).
- ¹²R. García, C. J. Gómez, N. F. Martínez, S. Patil, C. Dietz, and R. Magerle, *Phys. Rev. Lett.* **97**, 016103 (2006).
- ¹³N. F. Martínez, S. Patil, J. R. Lozano, and R. Garcia, *Appl. Phys. Lett.* **89**, 153115 (2006).
- ¹⁴U. Dietrich, M. Hackmann, B. Rieger, M. Klinga, and M. Leskelä, *J. Am. Chem. Soc.* **121**, 4348 (1999).
- ¹⁵S. Scherdel, S. Wirtz, N. Rehse, and R. Magerle, *Nanotechnology* **17**, 881 (2006).
- ¹⁶C. Dietz, S. Röper, S. Scherdel, A. Bernstein, N. Rehse, and R. Magerle, *Rev. Sci. Instrum.* **78**, 053703 (2007).
- ¹⁷A. Sakai, K. Tanaka, Y. Fujii, T. Nagamura, and T. Kajiyama, *Polymer* **46**, 429 (2005).
- ¹⁸A. Knoll, R. Magerle, and G. Krausch, *Macromolecules* **34**, 4159 (2001).